NWP SAF

Satellite Application Facility *for Numerical Weather Prediction*

Document NWPSAF-KN-TR-020
Version 1.0
October 2008

AWDP 1.0 validation

Jur Vogelzang, Anton Verhoef and Ad Stoffelen

KNMI, De Bilt, the Netherlands


AWDP 1.0 validation

KNMI, De Bilt, the Netherlands

This documentation was developed within the context of the EUMETSAT Satellite Application Facility on Numerical Weather Prediction (NWP SAF), under the Cooperation Agreement dated 16 December, 2003, between EUMETSAT and the Met Office, UK, by one or more partners within the NWP SAF. The partners in the NWP SAF are the Met Office, ECMWF, KNMI and Météo France.

Change record				
Version	**Date**	**Author**	**Approved**	**Remarks**
0.1	May 2008	Jur Vogelzang		First draft
0.2	June 2008	Jur Vogelzang		Added chapter 3
0.3	July 2008	Jur Vogelzang		Extended chapter 3
0.4	August 2008	Jur Vogelzang		Reorganized chapter 3
1.0	October 2008	All		Version for AWDP review

Contents

1 Introduction

1.1 Background

The ASCAT Wind Data Processor (AWDP) generates ocean vector wind fields from the measurements of the ASCAT scatterometer carried by MetOp-A or the Active Microwave Instrument (AMI) on the ERS 1 and 2 satellites. After the wind inversion and quality control steps, it allows performing the Ambiguity Removal with the Two-dimensional Variational Ambiguity Removal (2DVAR) method and it supports the Multiple Solution Scheme (MSS). The output of AWDP consists of wind vectors which represent surface winds within the ground swath of the scatterometer. Input of AWDP is Normalized Radar Cross Section (NRCS, σ_0) data. These data may be real-time. Moreover, AWDP needs Numerical Weather Prediction (NWP) model winds as a first guess for the Ambiguity Removal step. More information about the AWDP software package can be found in [*Verhoef et. al.,* 2007].

AWDP is to a large extent based on existing software that has been readily available in the so-called genscat library which was developed at KNMI in the framework of the NWP SAF and the Ocean and Sea Ice (OSI) SAF projects. Hence, AWDP shares much of its code with the SeaWinds Data Processor (SDP) software that is also a deliverable in the NWP SAF. Many of the SDP and AWDP developments are inherited from older software such as the QuikSCAT Data Processor (QDP) and Prescat (ERS scatterometer processing software).

1.2 Aims and scope

The aim of this report is to provide validation information about the ASCAT wind products that are generated by AWDP. The AWDP Test Report [*Verhoef et. al.,* 2008] provides information about the technical and functional tests that were carried out on the AWDP software; this report focuses more on the quality of the resulting wind product. Part of the AWDP functionality is already covered by the OSI SAF ASCAT Calibration and Validation Report [*Verspeek et. al.,* 2008], which mainly focuses on the wind inversion part of AWDP.

One aspect that is not covered by the available documents is the Ambiguity Removal part, i.e., the process of selecting the appropriate wind vector at each WVC from a set of ambiguous wind solutions that are provided by the wind inversion step. Like in SDP, the Ambiguity Removal is done by a 2DVAR algorithm, but its settings are optimized for ASCAT. The possibility to change the batch grid size and dimension offers a whole range of new settings for 2DVAR. The optimum settings will be determined in this report.

Note that in this report only the 25-km ASCAT product is considered. The quality of the 12.5-km product will be assessed in a later stage.

1.3 Outline of this report

Chapter 2 deals with the settings of the 2DVAR batch grid (resolution and size) and their influence on the AWDP wind product quality. Both statistical results and case studies are presented. In Chapter 3, some validation results from buoy and NWP model comparisons are presented. Also the influence of applying MSS is discussed.

Appendix A contains a list of software used to produce the figures in this report. Appendix B contains a list of abbreviations and acronyms.

2 2DVAR batch grid

2.1 Definitions

A complete description of 2DVAR is given in [*Vogelzang*, 2007], but in order to understand the next section of this chapter, some basic definitions and relations pertaining to the 2DVAR batch grid will be given here.

The basic quantity is the batch grid size Δ. It can be set to 100000 m (100 km, default in AWDP 1.0 and older), 50000 m (50 km), or 25000 m (25 km). The 2DVAR batch grid is a square grid, so its grid size is Δ in both directions.

The next important quantity is the observation sampling R. In AWDP 1.0, R can have the values 25 km and 12.5 km, with the restriction $R \leq \Delta$. If $R = \Delta$, all observations coincide with batch grid cells. If $R < \Delta$ the analysis is given on a coarser grid than the observations, so the analysis must be interpolated at some of the observation points. The number of wind vector cells (WVCs) per row is 42 for 25 km sampling, 21 WVCs to the left of the satellite ground track and 21 to the right, with a gap of 766 km between the left and right swath (assuming a minimum incidence angle of 25° for the mid-beams and a satellite altitude of 822 km). In 2DVAR the two swaths are processed separately, so the swath width S is 525 km.

Since the background part of the cost function is evaluated in the frequency domain rather than the spatial domain, the analysis increments on the 2DVAR batch grid must go to zero at the edges of the grid. Therefore a free edge is added around the batch grid. As a result, the observations are embedded in a larger grid. The size of the free edge is m grid points, so its spatial extension is $E = m\Delta$. This fixes N, the number of batch grid cells in the across track direction as

$$N = \frac{S + 2E}{\Delta} = \frac{S}{\Delta} + 2m \,. \tag{2.1}$$

The ASCAT level 1 data are disseminated as BUFR files containing 3 minutes of data, or 48 rows at 25 km resolution. Therefore the part of the orbit being processed sizes T = 1200 km. This fixes M, the number of batch grid cells in the along track direction as

$$M = \frac{T + 2E}{\Delta} = \frac{T}{\Delta} + 2m \,. \tag{2.2}$$

Note that AWDP 1.0 has Δ = 100 km and m = 5, so N should be equal to 16 and M should be equal to 22. Since the original FFT algorithm in 2DVAR requires the number of batch grid cells in both directions to be a power of 2, N is set to 32. This means that the number of free cells on the right hand side equals 21 and on the top side 15 rather than 5.

2.2 Batch grid size

The first step is to determine the optimal batch grid size Δ. It has a default value of 100 km, but at 25 km resolution its value could also be 50 km or 25 km. All ASCAT 25-km data from January 2008 were processed for Δ equal to 100 km, 50 km, and 25 km. The standard 2DVAR settings were applied and a free edge of 1800 km at least was chosen. Table 2.1 gives the 2DVAR batch grid parameters for these three runs. In some cases the dimension of the batch grid is slightly increased in order to avoid odd numbers or even numbers with large prime factors in the FFT routine.

Run id.	Δ (km)	Batch grid dimension	Free edge (points)
D100_E1800	100	42 × 48	18
D050_E1800	50	84 × 96	36
D025_E1800	25	168 × 192	72

Table 2.1 Batch grid parameters.

The zonal and meridional wind speed components, *u* and *v*, were calculated for each wind vector cell (WVC) and the statistics of their differences were calculated. The results are listed in table 2.2.

Grid size (km)		Zonal component *u* (m/s)				Meridional component *v* (m/s)			
Δ_1	Δ_2	bias	σ	min	max	bias	σ	min	max
100	50	+0.00009	0.18	-17.9	+24.2	+0.00035	0.16	-17.1	+16.3
100	25	+0.00009	0.19	-17.9	+26.1	+0.00039	0.16	-17.7	+16.4
50	25	-0.00002	0.094	-15.0	+24.7	+0.00004	0.062	-15.1	+14.8

Table 2.2 Statistics of the wind field comparison for various batch grid sizes.

Table 2.2 shows that the bias and the standard deviation σ are small, notably for the difference between the results with Δ = 50 km and those with Δ = 25 km, but that some large differences remain. The maximum differences in *u* between grid sizes of 100 km and 25 km occur on January 3 between 15:33 and 15:36 UTC in orbit 6264 (file ascat_20080103_153303_metopa_06264…). The results in table 2.2 obtained for Δ = 25 km differ little from those for Δ = 50 km. These results indicate that the optimum 2DVAR batch grid size is 50 km for ASCAT at 25 km resolution. Note that the same value has been found for SeaWinds at the same resolution [*Vogelzang,* 2008].

Figure 2.1 shows the area of maximum difference in *u*. It lies south of Australia close to the Antarctic coast. WVCs rejected by the MLE flag (KNMI Quality Control) are depicted in orange, those rejected by the VarQC flag in purple. The ECMWF model (upper left panel in figure 2.1 shows a strong westerly wind south of a low pressure area, the centre of which is not visible in this batch. The batch contains a small number of observations. Note that the singular anomalous ice points close to the Antarctic coast are screened out effectively by the MLE flag. In the current AWDP these point do not occur any more after inversion.

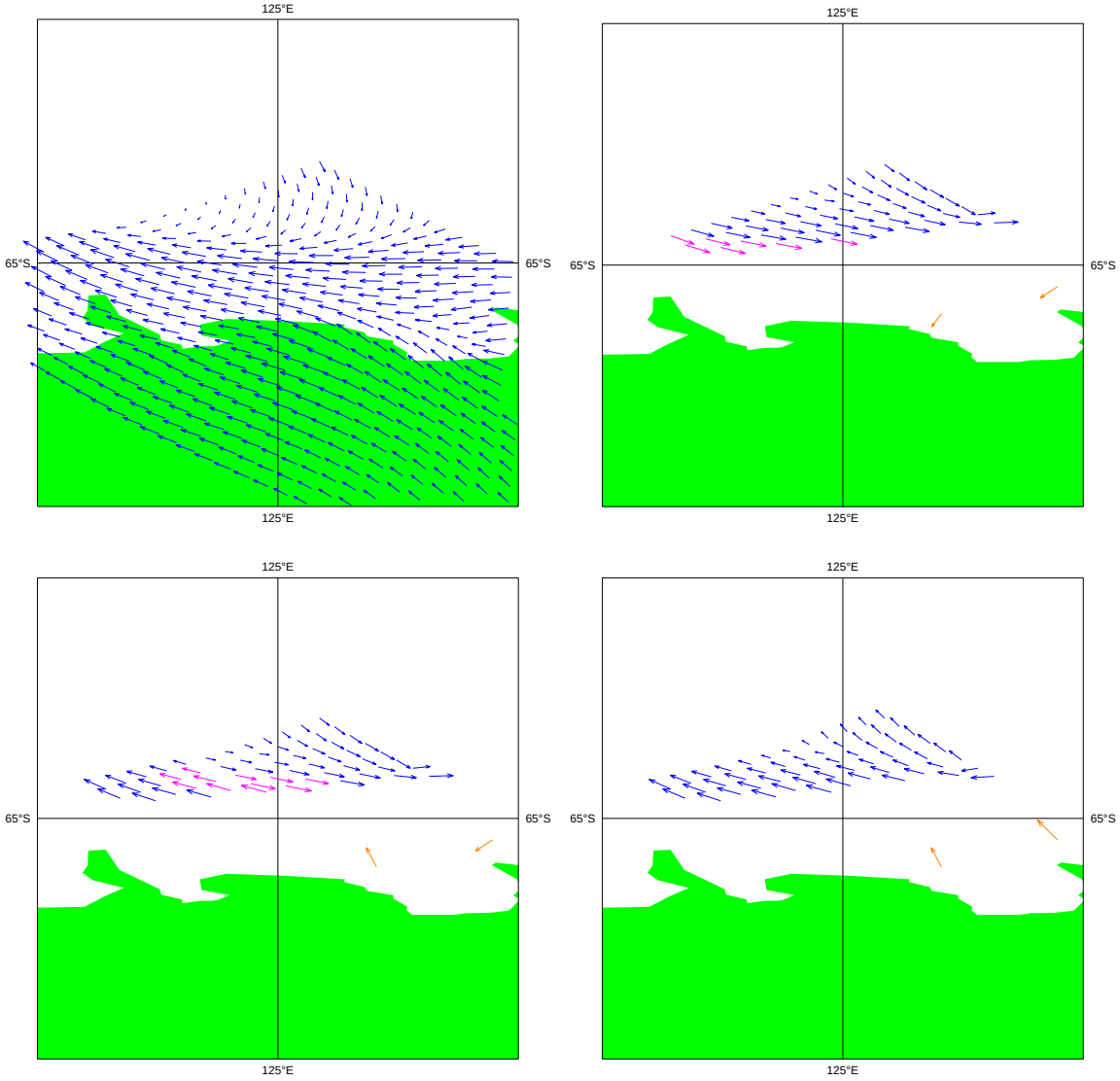

Figure 2.1 Area of maximum difference in *u*. Upper left: ECMWF background; upper right: AWDP result with 100 km batch grid size; lower left: AWDP result with 50 km batch grid size; lower right: AWDP result with 25 km batch grid size. Orange arrows are flagged by the KNMI QC procedure; purple arrows by VarQC.

With 100 km batch grid size (upper right panel in figure 2.1) the wind direction is obviously wrong all over the batch. With 50 km batch grid size the situation improves slightly: the wind direction in the western part of the batch is now correct, but in the eastern part it is still wrong. The best results are obtained with 25 km batch grid size. The strong westerly winds are more or less reproduced, but the directions at the northeastern edge still deviate from the background and fail to reproduce the wind structure of the low.

The minimum difference in *u* occurs on January 9 between 01:45 and 01:48 UTC in orbit 6341 (file ascat_20080109_014501_metopa_06341…). Figure 2.2 shows the results of this batch. It lies in the Atlantic east of Argentina. The ECMWF background (upper left panel) shows a complicated wind pattern with several strong convergences. With 100 km batch grid size (upper right panel) the wind direction is wrong in a large area between 60° W and 65° W and between 48° S and 50° S. At 50 km (lower left panel) and 25 km (lower right panel) batch grid size, the area is split in two

smaller parts. Though the directional mismatch between background and observation is reduced, there is still a large discrepancy. This case will be studied later when the 2DVAR error model parameter settings are studied in more detail.

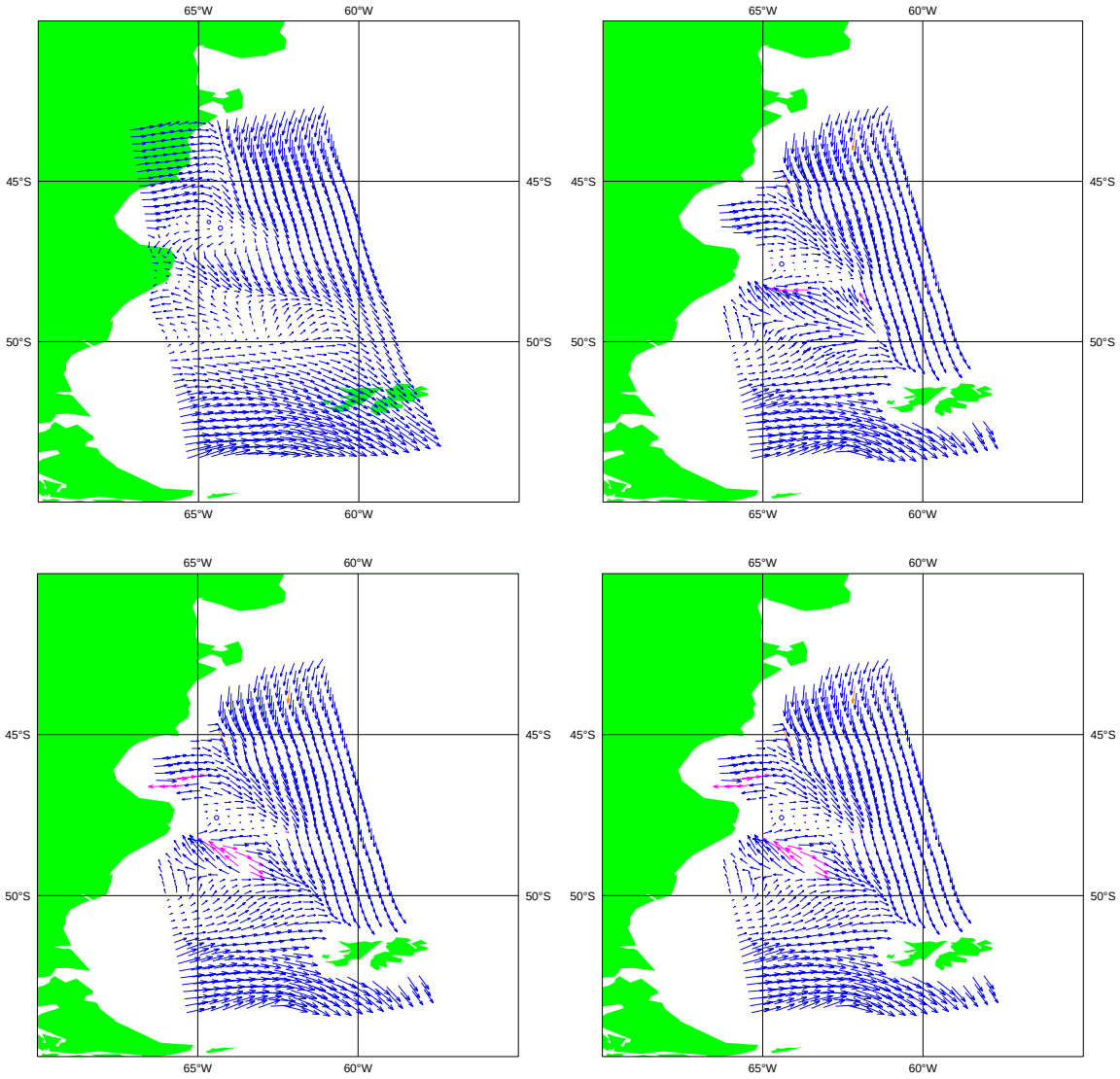

Figure 2.2 Area of minimum difference in *u*. Upper left: ECMWF background; upper right: AWDP result with 100 km batch grid size; lower left: AWDP result with 50 km batch grid size; lower right: AWDP result with 25 km batch grid size. Orange arrows are flagged by the KNMI QC procedure; purple arrows by VarQC.

2.3 Free edge size

In the previous section it was shown that the optimum batch grid size is 50 km. The next step is to determine the optimum size of *E*, the free edge around the 2DVAR batch grid. All data from January 2008 were processed for *E* equal to 1200 km, 1800 km, and 2400 km. The standard 2DVAR settings were applied, and table 2.3 gives the 2DVAR batch grid parameters for these three runs.

Run id.	*E* (km)	Batch grid dimension	Free edge (points)
D050_E1200	1200	60 × 72	24
D050_E1800	1800	84 × 96	36
D050_E2400	2400	108 × 120	48

Table 2.3 Batch grid parameters.

In some cases the dimension of the batch grid is slightly increased in order to avoid large prime factors in the FFT routine. The zonal and meridional wind speed components, *u* and *v*, were calculated for each wind vector cell (WVC) and the statistics of their differences were calculated as in the previous section. The results are listed in table 2.4.

Free edge (km)		Zonal component *u* (m/s)				Meridional component *v* (m/s)			
		Bias	σ	min	max	bias	σ	min	Max
2400	1800	+0.00002	0.044	-24.7	+13.7	+0.00009	0.046	-13.6	+15.9
2400	1200	-0.00004	0.099	-24.7	+15.1	-0.00020	0.103	-16.4	+14.1
1800	1200	-0.00005	0.089	-13.6	+15.1	-0.00030	0.104	-16.4	+14.1

Table 2.4 Statistics of the wind field comparison for various free edge sizes.

Table 2.4 shows that the results for the difference between $E = 2400$ km and $E = 1800$ km are closer to each other than their differences with $E = 1200$ km. This is also similar as found for SDP. The minimum difference in *u* occurs for the same batch as in the previous section. The maximum difference in *v* occurs on January 19 between 11:09 and 11:12 UTC in orbit number 6489, file ascat_20080119_110902_metopa_06489… The area, shown in figure 2.3, lies in the Equatorial Atlantic. The ECMWF background wind field (upper left panel) shows a smooth wind field with some convergence in the northern part. The AWDP results with free edge size 2400 km (upper right panel), 1800 km (lower left panel) and 1200 km (lower right panel) show an extensive MLE QC area. Around this area, the wind tends to orientate either parallel or perpendicular to the satellite moving direction. The WVC causing the largest difference in *v* lies east of the QC area and switches direction at free edge size 1800 km.

The scatterometer wind vectors in the whole area above the equator look suspicious, and more detailed investigation is needed to resolve these difficulties.

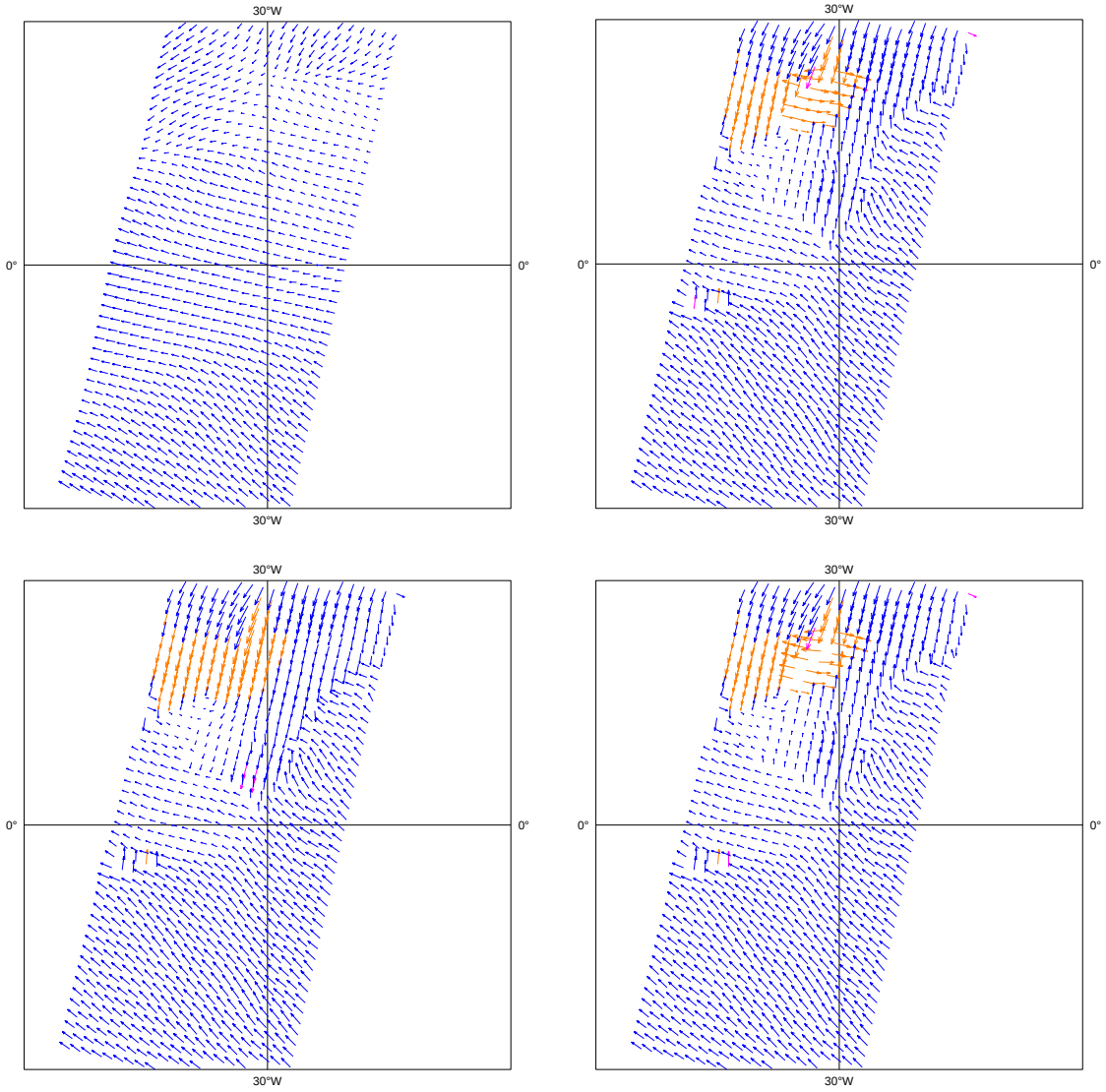

Figure 2.3 Area of maximum difference in *v*. Upper left: ECMWF background; upper right: AWDP result with 2400 km free edge; lower left: AWDP result with 1800 km free edge; lower right: AWDP result with 1200 km free edge. Orange arrows are flagged by the KNMI QC procedure; purple arrows by VarQC.

3 Validation

3.1 Comparison with model winds and buoys

Figure 3.1 shows the standard deviation of the difference between the ASCAT wind and the ECMWF background for *u* and *v* as a function of WVC number. AWDP was run on all data from January 2008 with 50 km batch grid size and 1800 km free edge size. No MSS was applied.

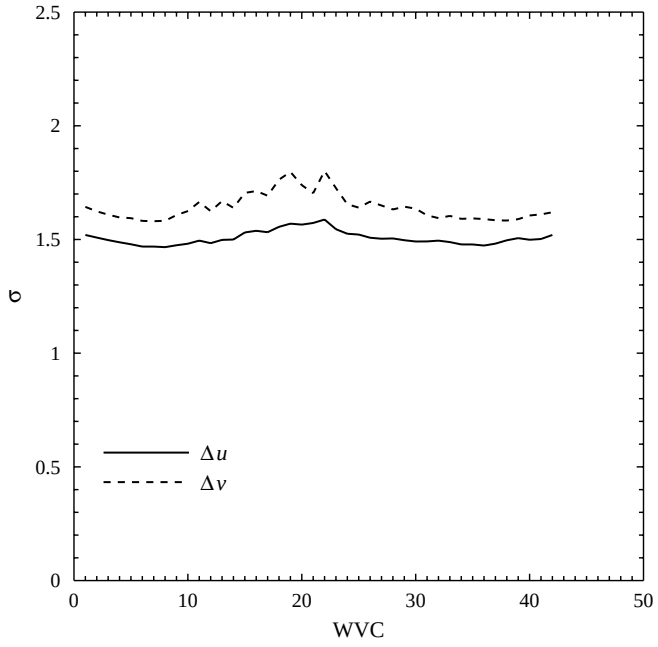

Figure 3.1 Standard deviation of the difference between the ASCAT winds and the ECMWF background for the components *u* (solid curve) and *v* (dashed curve) as a function of WVC number.

Figure 3.1 shows that the standard deviation of the difference is between 1.4 and 1.6 m/s for *u*. It is slightly higher, between 1.6 and 1.8 m/s, for *v*. The standard deviation of the wind component difference shows little variation over the swath, though there is a slight increase around WVC 21-22 (low incidence angles) and at the edges (high incidence angles).

Table 3.1 shows the comparison with available wind measurements from moored buoy as obtained from [*OSI SAF ASCAT 25-km buoy validations*]. Only buoys with reliable performance were selected, resulting in a total number of over 2100 collocated measurements from 129 different buoys over January 2008. The buoys are located in the tropical oceans and along the coast of Europe and North America. A measurement is considered as collocated if the time between ASCAT and buoy measurement is less than 30 minutes and their distance is less than 25 km divided by $\sqrt{2}$.

	Buoys	ECMWF
σ_u (m/s)	1.87	1.48
σ_v (m/s)	1.89	1.63

Table 3.1 Comparison of ASCAT winds with buoy measurements (~2100 collocations) and ECMWF background (all WVCs).

Table 3.1 shows that averaged over all WVCs the ASCAT winds compare slightly better to the ECMWF background than to the buoy measurements.

3.2 Effect of MSS

Table 3.2 shows the effect of MSS on the difference between the AWDP wind fields and the ECMWF background. Since MSS avoids the selection of ad hoc local solution minima and allows 2DVAR to choose from 144 ambiguities, it is more likely that application of MSS reduces the standard deviation of the wind differences. Table 3.2 shows that this is indeed the case, notably for the meridional component *v*.

	σ_u (m/s)	σ_v (m/s)
No MSS	1.51	1.65
MSS	1.40	1.39

Table 3.2 Standard deviation of the difference between the AWDP wind and the ECMWF background.

Figure 3.2 shows the area of minimum difference in v between AWDP with or without MSS and the ECMWF background. The minimum difference Δv equals -23.0 m/s and occurs on January 20, 2008 around 22:24 UTC for orbit 6510 (file ascat_20080120_222400_metopa_06510…). The upper left panel of figure 3.2 shows the AWDP wind field without MSS, the upper right panel the AWDP wind field with MSS, and the lower panel the ECMWF background. The minimum difference occurs near a cyclone that has different positions in the ASCAT measurements and the ECMWF background. Because of large differences between measurement and background, some WVCs have their VarQC flag set (purple arrows). There is also some QC around the centre of the cyclone and more to the southwest of it, as indicated by the orange arrows. Note that with MSS the wind field around the cyclone is smoother than without. MSS allows 2DVAR to choose from 144 ambiguities. It is therefore more likely that 2DVAR with MSS will select a solution with somewhat lower a-priori probability but in closer comparison to its neighbours and the background, yielding lower cost function values (and therefore less WVCs with the VarQC flag set). For example, in the case shown the background differs significantly from the observation. Apparently, the smoothing properties of MSS depend on the structure functions used in this case.

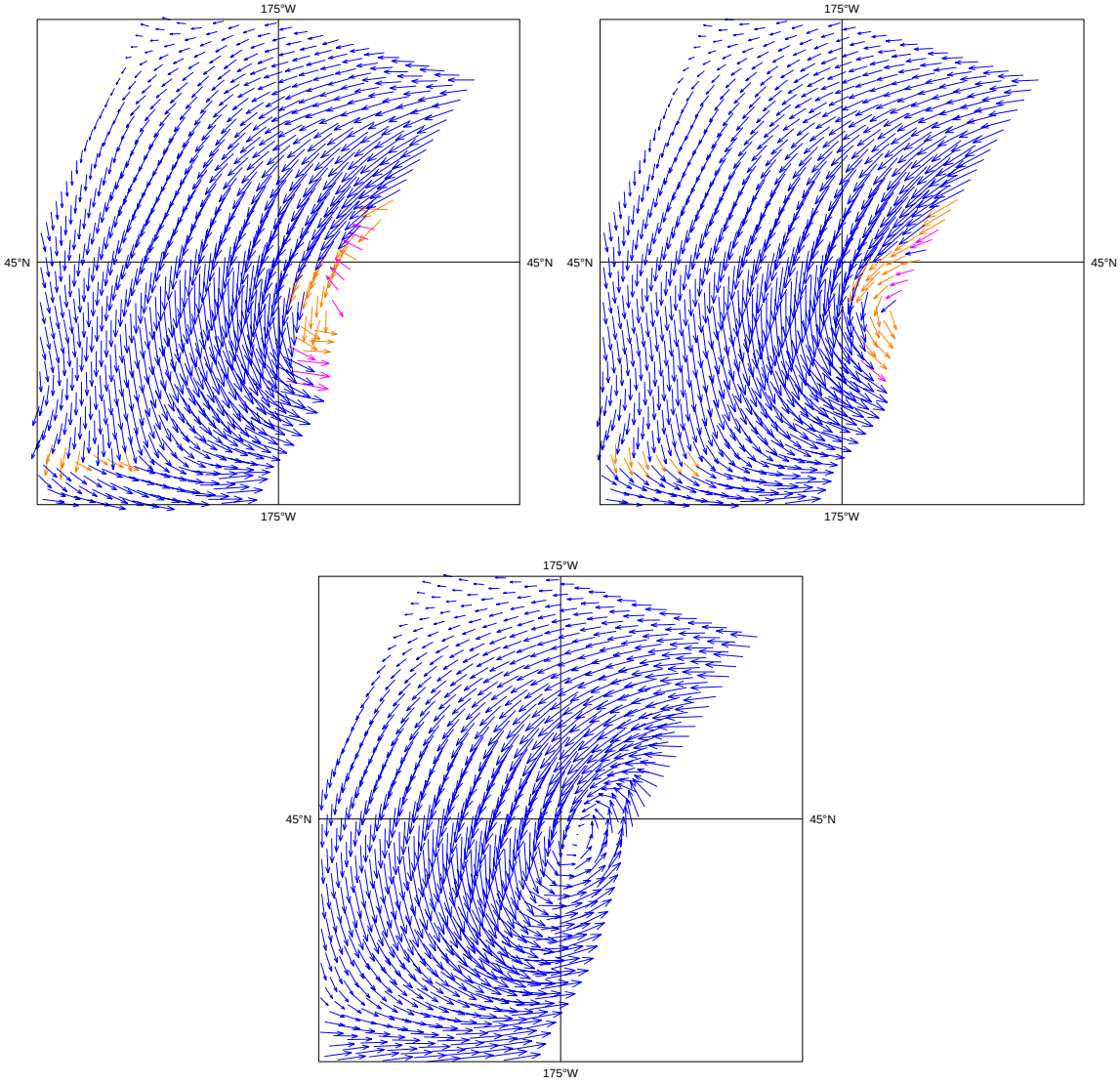

Figure 3.2 Area where the minimum difference in zonal wind component occurs. Upper left: AWDP without MSS; upper right: AWDP with MSS; lower: ECMWF background.

Figure 3.3 shows the area of maximum difference, $\Delta v = 22.4$ m/s, obtained on January 19, 2008 around 14:24 UTC (file ascat_20080119_142402_metopa_06491…). Orange arrows indicate WVCs with the KNMI QC flag set; purple arrows WVCs with the VarQC flag set. As in figure 3.2, there is disagreement between background and observations in figure 3.3: the ECMWF background shows a front in the northwestern corner that is absent in the AWDP results with or without MSS.

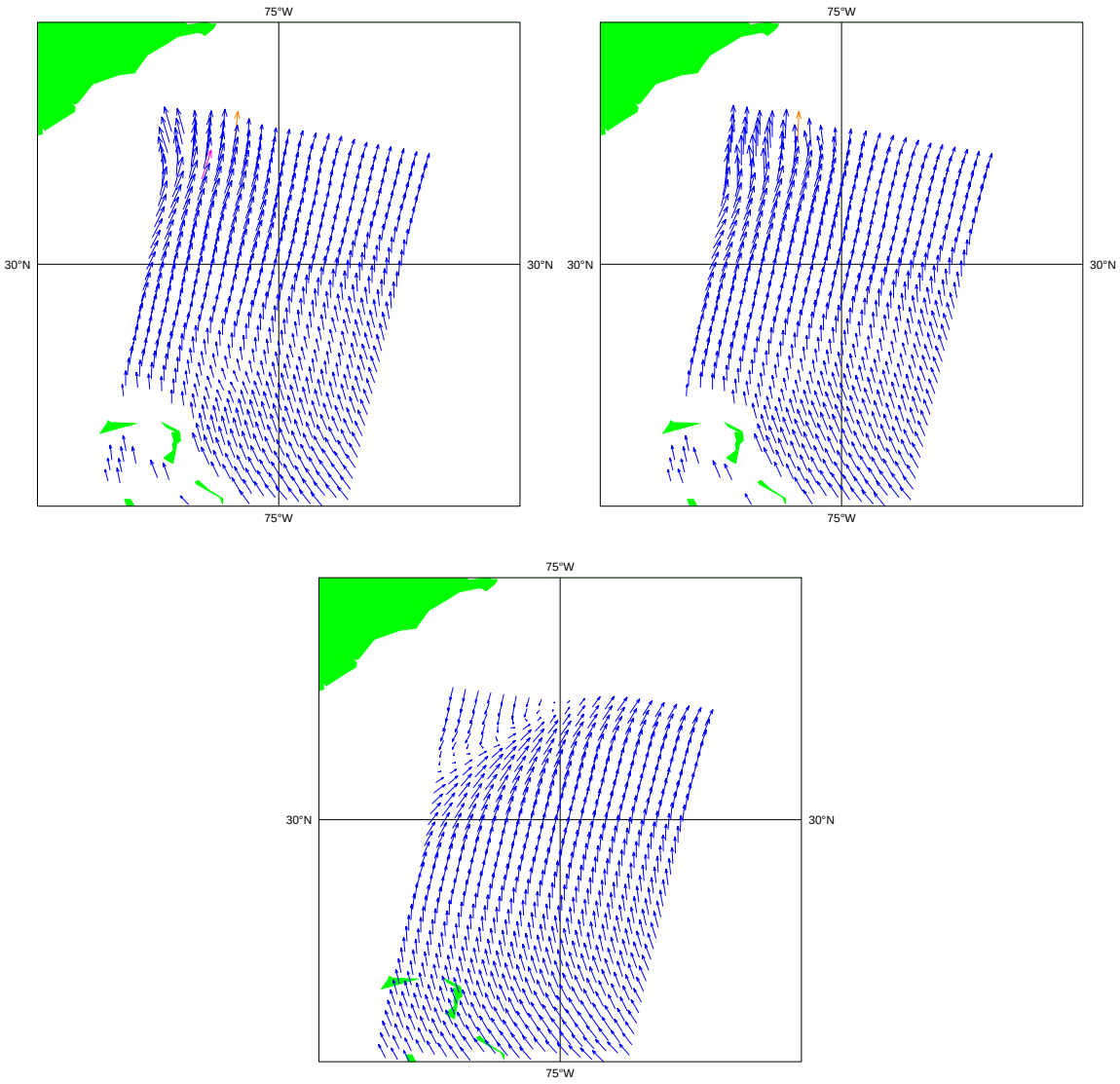

Figure 3.3 Area where the maximum difference in zonal wind component occurs. Upper left: AWDP without MSS; upper right: AWDP with MSS; lower: ECMWF background.

3.3 Covariance and spectrum

The covariance or the autocorrelation (normalized covariance) gives more insight in the information content of scatterometer and model winds, and is useful in detecting white noise [*Vogelzang*, 2006]. Figure 3.4 shows the covariance as a function of distance for the ECMWF background (dashed curves) and AWDP (solid curves) with MSS (upper panels) or without MSS (lower panels). Blue curves represent results for the zonal component *u*; red curves for the meridional component *v*.

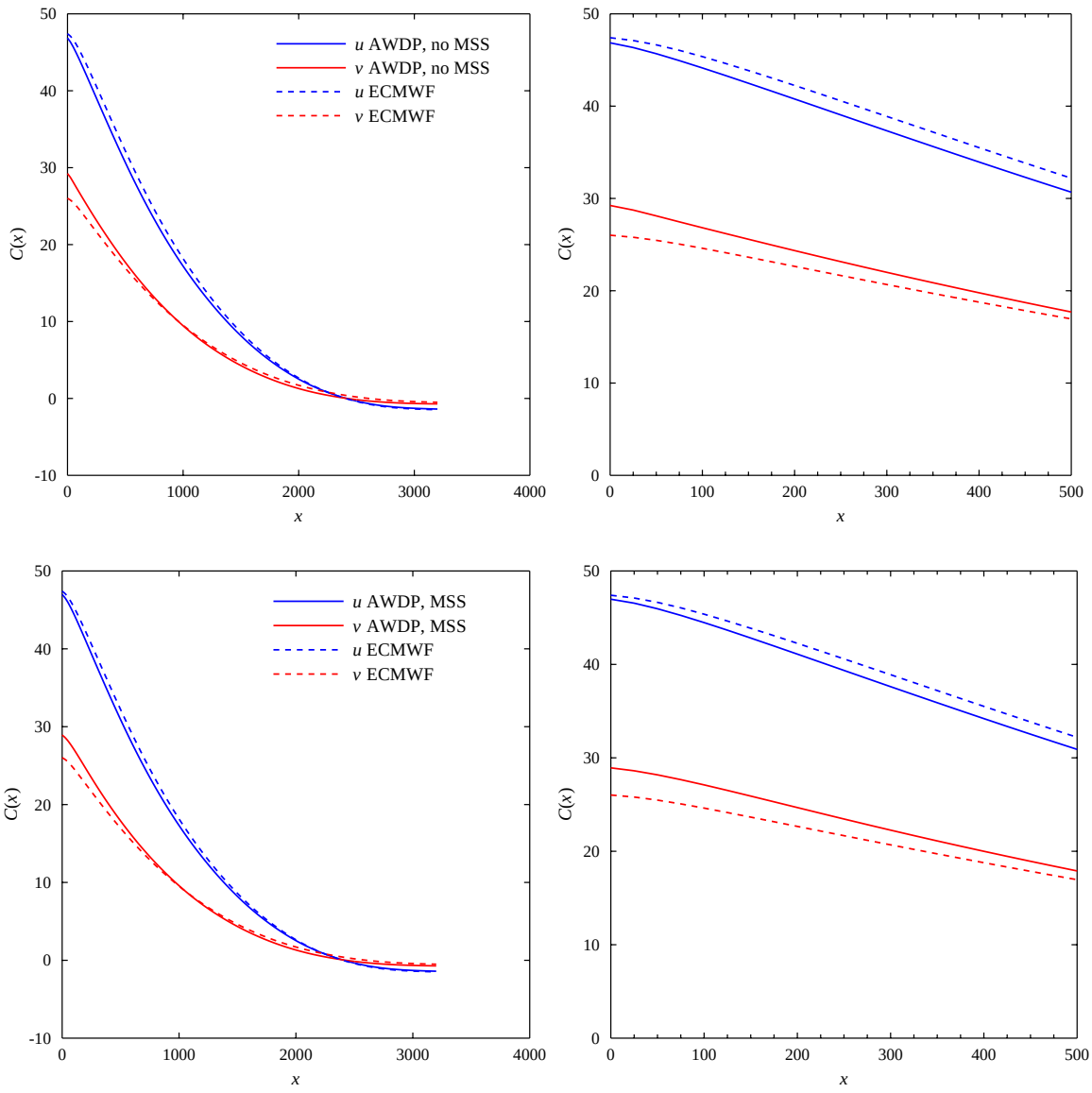

Figure 3.4 Covariance for the zonal and meridional wind components obtained using the ECMWF model and AWDP with MSS (upper panels) or without MSS (lower panels). The right hand panels are enlargements at small distances.

Application of the MSS has very little effect on the resulting covariances. The striking feature in figure 3.4 is the relatively large difference in covariance at small distance between the scatterometer and background meridional wind component *v*. At zero distance the covariance equals the variance, and the distance can not be explained by the standard deviations listed in table 3.2.

This is made clearer by figure 3.5 which shows the variance of the selected wind components, the model wind components, and their difference. The left hand panel of figure 3.5 is without MSS, the right hand panel with MSS.

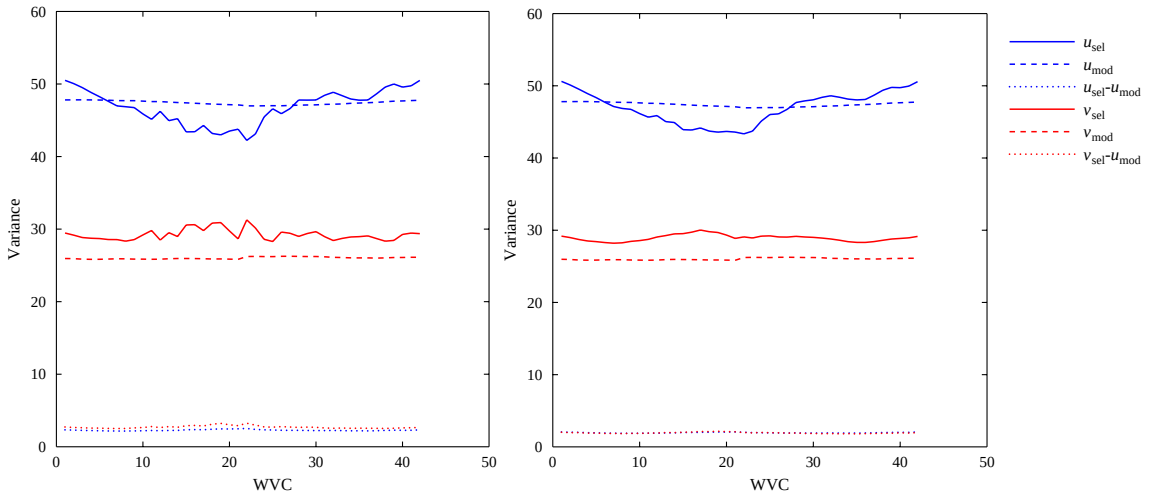

Figure 3.5 Variances as a function of WVC number for various wind components without MSS (left) and with MSS (right)

Figure 3.5 shows that the variance in the scatterometer wind components vary considerably with WVC number, while those for the model wind components and the differences are relatively constant. Application of MSS smoothens the curves, but preserves their large-scale variation.

The discrepancy in figure 3.5 is not caused by the fact that AWDP at low wind speeds tends to align the wind vectors parallel or perpendicular to the midbeam direction, because restriction of the AWDP selected wind speed to values above 4 m/s have little effect on the variances (no results shown).

Figure 3.6 shows the autocorrelation (left) and the spectrum (right) for the zonal and meridional wind components, *u* and *v* of all ASCAT data of January 2008 processed with AWDP without MSS. Figure 3.6 shows that the autocorrelation for ASCAT winds smoothly approaches unity for small distances. This indicates that there is little or no white noise in the ASCAT data. The curves for the ASCAT winds (solid) lie below those of the ECMWF model (dashed), indicating that the scatterometer shows more small scale features than the model as expected. This is corroborated by the spectrum in the right hand panel of figure 3.6. At low spatial frequencies (large spatial scales) the information content in ASCAT and ECMWF wind fields is equal. At smaller scales, the ASCAT winds contain more information.

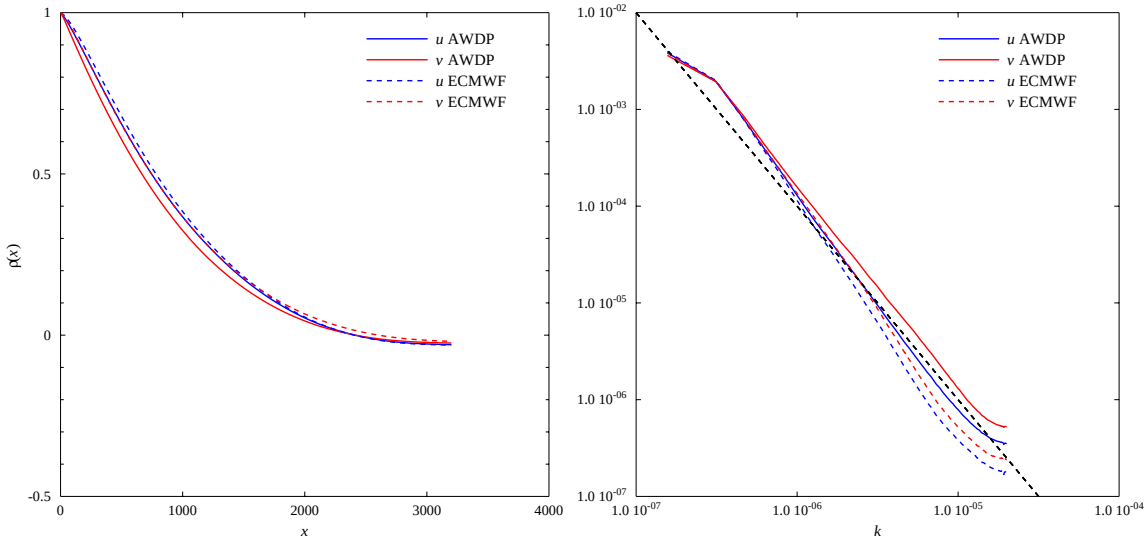

Figure 3.6 Autocorrelation (left) and spectrum (right) for all ASCAT data from January 2008 and the corresponding ECMWF model predictions. The black dashed curve in the right hand panel gives a k^{-2} spectrum.

3.4 Selection probabilities

2DVAR uses spatial as well as statistical consistency for selecting the ambiguity that is most likely the true wind [*Vogelzang*, 2007]. This means that the a-priori probability of each ambiguity, P, derived from the distance between the scatterometer measurement and the Geophysical Model Function, should affect the selection process. Figure 3.7 shows $p(\mathrm{Sel} \mid P)$, the conditional probability that an ambiguity is selected provided that its a-priori probability equals P. The curves in figure 3.7 are normalized to one, so they can be interpreted as probability density functions (pdf). For perfect statistical consistency

$$p(\mathrm{Sel} \mid P) = 2P \quad , \tag{3.1}$$

and this is shown as the black dashed curve in figure 3.7

The left hand panel of figure 3.7 shows the results without MSS. Both 2DVAR (solid blue curve) and closest-to-background (dotted red curve) are close to statistical consistency. The difference between the two curves is very small and therefore almost indiscernible in figure 3.7. Using first rank as ambiguity removal method results in a curve much further from perfect statistical consistency. Since AWDP without MSS usually returns two ambiguities, the first rank result starts at $P = 0.5$ and becomes constant for $P > 0.5$. These results resemble those for SDP, though AWDP deviates slightly more from perfect statistical consistency.

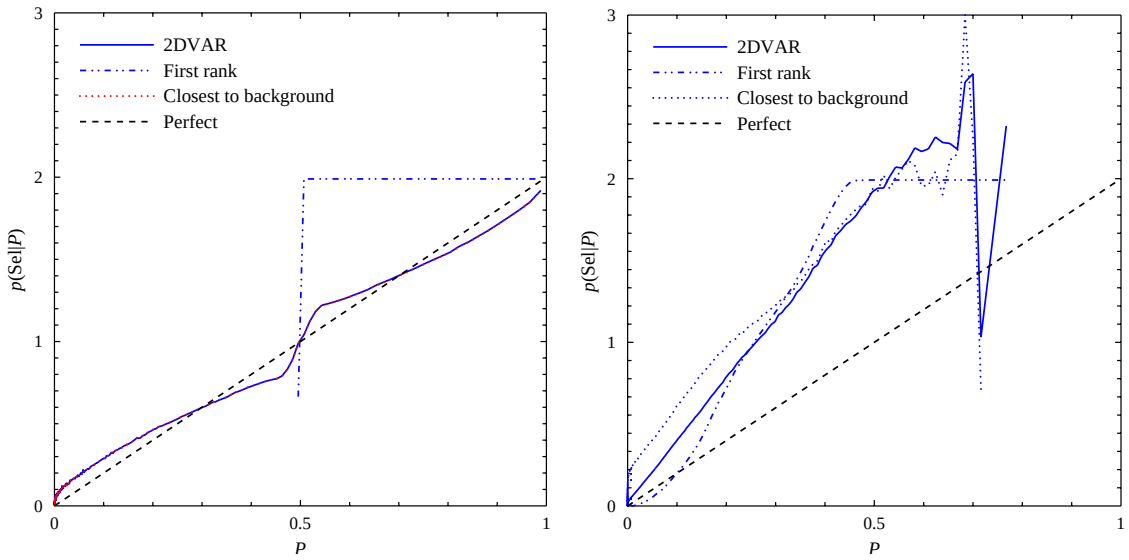

Figure 3.7 Conditional pdf's of the selection probability as a function of the a priori probability P for three ambiguity removal methods. Left: without MSS; right: with MSS. The curves labeled "Perfect" indicate perfect statistical consistency.

The right hand panel of figure 3.7 shows the results with MSS. Because a-priori probabilities larger than about 0.7 do not occur in the dataset, the curves end here and become rather noisy close to this threshold. As without MSS, the first rank probability becomes constant for $P \geq 0.5$.2DVAR and closest-to-background gives similar results, though the 2DVAR result behaves more like a straight line for $P < 0.5$ and is therefore closer to perfect statistical consistency.

To further investigate the value added by 2DVAR over the simple closest-to-background method, the cases were studied in which 2DVAR without MSS selects an other solution than closest-to-background. The results are listed in table 3.3. In most cases the a-priori probability P is 0.5, and the difference is caused by the structure functions in 2DVAR. In the remaining cases where the two ambiguities have different a priori probability, 2DVAR has a slight tendency to select the ambiguity with highest a-priori probability. The average a-priori probability over all cases is 0.506 for 2DVAR and 0.496 for closest-to-background. These figures indicate little effect of 2DVAR.

Equal values for P	157461
2DVAR selects highest P	26209
2DVAR selects lowest P	21282

Table 3.3 Statistics for the selection in cases 2DVAR and closest-to-background select a different ambiguity.

References

- OSI SAF ASCAT 25-km buoy validations
  See link 'Buoy validations' on www.knmi.nl/scatterometer/ascat_osi_25_prod/
- Verhoef, A., Vogelzang, J., Verspeek, J. and Stoffelen, A., 2007
  AWDP User Manual and Reference Guide, Report NWPSAF-KN-UD-005, UKMO, UK
- Verhoef, A., Vogelzang, J., Verspeek, J. and Stoffelen, A., 2008
  AWDP Test Report, Report NWPSAF-KN-TV-005, UKMO, UK
- Verspeek, J., Portabella, M., Stoffelen, A., and Verhoef, A., 2008
  Calibration and Validation of ASCAT Winds, Report SAF/OSI/KNMI/TEC/TN/163
- Vogelzang, J., 2006,
  On the quality of high resolution scatterometer wind fields, Report NWPSAF-KN-TR-002, UKMO, UK, www.metoffice.gov.uk/research/interproj/nwpsaf/scatterometer/index.html
- Vogelzang, J., 2007,
  Two dimensional variational ambiguity removal, Report NWPSAF-KN-TR-004, UKMO, UK. www.metoffice.gov.uk/research/interproj/nwpsaf/scatterometer/index.html
- Vogelzang, J., 2008,
  SDP 2.0 validation, Report NWPSAF-KN-TR-007, UKMO, UK,
  www.metoffice.gov.uk/research/interproj/nwpsaf/scatterometer/index.html

Appendix A Software used

Tables A.1 and A,2 show for each table and figure of this report, respectively, the name of the program that generated the data and the name of the program that made the plot. All programs (with the exception of PWFX which uses ECMWF's MAGICS library) are under version control of the KNMI CVS repository, so they can always be retrieved if necessary.

Table	Generating program
2.2	genscat/tools/swat/DSW
2.4	genscat/tools/swat/DSW
3.1, 3.2	genscat/tools/swat/DSW
3.3	genscat/tools/sba/SBA

Table A.1 Generating and plotting programs for the figures in this report.

Figure	Generating program	Plotting program
2.1-2.3	AWDP 1.0	PWFX (not in genscat)
3.1	genscat/tools/swat/DSW	genscat/tools/swat/PDN
3.2-3.3	AWDP 1.0	PWFX (not in genscat)
3.4-3.5	genscat/tools/sba/SBA	genscat/tools/sba/SBP
3.6	genscat/tools/sac/SAC	genscat/tools/sac/PAC
3.7	genscat/tools/sba/SBA	genscat/tools/sba/SBP

Table A.2 Generating and plotting programs for the figures in this report.

Appendix B Abbreviations

Name	Description
2DVAR	Two Dimensional Variational Ambiguity Removal
AMI	Active Microwave Instrument, scatterometer on ERS-1 and ERS-2 satellites
AR	Ambiguity Removal
ASCAT	Advanced SCATterometer on MetOp
AWDP	ASCAT Wind Data Processor
ERS	European Remote Sensing satellites
ECMWF	European Centre for Medium-range Weather Forecasts
EUMETSAT	European Organization for the Exploitation of Meteorological Satellites
FFT	Fast Fourier Transform
genscat	generic scatterometer software routines
GMF	Geophysical model function
KNMI	Koninklijk Nederlands Meteorologisch Instituut (Royal Netherlands Meteorological Institute)
MetOp	Meteorological Operational Satellite
MLE	Maximum Likelihood Estimator
MSS	Multiple Solution Scheme
NRCS	Normalized Radar Cross-Section (σ_0)
NWP	Numerical Weather Prediction
OSI	Ocean and Sea Ice
pdf	probability density function
QC	Quality Control
RMS	Root Mean Square
SAF	Satellite Application Facility
WVC	Wind Vector Cell, also called node or cell